

Control and amplification of Bloch oscillations via photon-mediated interactions

Haoqing Zhang,^{1,2} Anjun Chu,^{1,2} Chengyi Luo ¹, James K. Thompson,¹ and Ana Maria Rey ^{1,2}

¹*JILA, NIST, and Department of Physics, University of Colorado, Boulder, Colorado 80309, USA*

²*Center for Theory of Quantum Matter, University of Colorado, Boulder, Colorado 80309, USA*



(Received 24 January 2023; accepted 7 August 2023; published 15 September 2023)

We propose a scheme to control and enhance atomic Bloch oscillations via photon-mediated interactions in an optical lattice supported by a standing-wave cavity with incommensurate lattice and cavity wavelengths. Our scheme uses position-dependent atom-light couplings in an optical cavity to spatially prepare an array of atoms at targeted lattice sites starting from a thermal gas. On this initial state we take advantage of dispersive position-dependent atom-cavity couplings to perform nondestructive measurements of single-particle Bloch oscillations, and to generate long-range interactions self-tuned by atomic motion. The latter leads to the generation of dynamical phase transitions in the deep lattice regime and the amplification of Bloch oscillations in the shallow lattice regime. Our work introduces possibilities accessible in state-of-the-art cavity QED experiments for the exploration of many-body dynamics in self-tunable potentials.

DOI: [10.1103/PhysRevResearch.5.L032039](https://doi.org/10.1103/PhysRevResearch.5.L032039)

I. INTRODUCTION

Bloch oscillations (BOs) [1] are center-of-mass oscillations or coherent breathing experienced by independent particles in a periodic lattice potential in the presence of a constant force (e.g., gravity). Although it has been hard to directly control BOs in conventional electron systems, they have been observed in tailored semiconductor systems [2] as well as ultracold atom systems trapped in optical lattices [3,4]. Nevertheless, for the latter, the lattice potential is by implementation rigid and therefore not a good test bed example of the underlying physics in real materials where the phonons of the crystal dynamically interact with the electron motion. Furthermore, interatomic interactions have always been a competing mechanism that damp the oscillations.

Here we propose a scheme to control and amplify atomic BOs via photon-mediated interactions in a gravity-tilted optical lattice supported by a standing-wave optical cavity with incommensurate lattice and cavity wavelengths. In our case, photons can actively modify the periodic potential experienced by the atoms and therefore resemble the role of phonons in a real solid-state environment. Even though experiments that track BOs in optical cavities have been implemented before using a Bose-Einstein condensate (BEC) [5–9], here we propose to use inhomogeneous atom-light couplings to prepare an array of atoms on specific lattice sites and initialize the dynamics [10]. This can be achieved via position-dependent dispersive atom-light couplings to map the motion of the atoms under BOs into the frequency shift of the cavity resonance. Our protocol not only avoids the ultracold

degenerate initial states required in nondestructive measurements of BOs, but also provides flexible self-tunability of the cavity-mediated long-range interactions by the atomic motion. Moreover, in contrast to prior experiments where the periodic potential was generated by the probe laser field itself [5–9] or separate probe field for site-independent atom-light coupling [11], we use an additional lattice potential that traps the atoms and controls the degree of delocalization of the underlying Wannier-Stark (WS) states [12] in our system. In this setting, different from the well-studied case of contact interactions [13–20], the photon-mediated interactions can modify BOs depending on the position of other atoms in the array. Taking advantage of this feature we show versatile many-body phenomena can be realized in different parameter regimes of this system: In the deep lattice region, we find dynamical phase transitions (DPTs) related to the Lipkin-Meshkov-Glick (LMG) model [21,22], which potentially enables rapid generation of spin-squeezed states [23–25] with WS states directly, bypassing the need for Raman transitions [12]. In the shallow lattice, we find the amplification of Bloch oscillation amplification originating from the pair production [26–29] process from the central to adjacent WS states. We also discuss feasible implementations in state-of-the-art cavity QED experiments [30,31].

II. MODEL

We consider an ensemble of N ultracold atoms with mass M trapped in a standing-wave optical cavity along the vertical direction \hat{z} as shown in Fig. 1(a). The atoms are confined in the lowest band of the one-dimensional (1D) optical lattice supported by the cavity, with local gravitational acceleration \vec{g} generating an additional Mgz potential between sites separated by a vertical distance z . Here we consider the pure 1D model for simplicity and discuss the modification by the radial modes in [32]. A single internal level $|g\rangle$ in the atomic

Published by the American Physical Society under the terms of the [Creative Commons Attribution 4.0 International](https://creativecommons.org/licenses/by/4.0/) license. Further distribution of this work must maintain attribution to the author(s) and the published article's title, journal citation, and DOI.

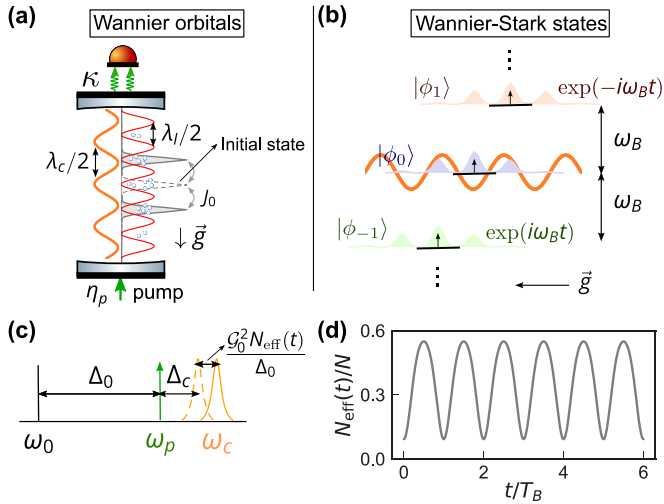


FIG. 1. Model system. (a) An ensemble of N atoms is trapped in the lowest band of an optical lattice supported by an optical cavity aligned with gravitational acceleration \vec{g} . Considering the atoms are initially localized in a Wannier orbital (gray dashed line), hopping to the nearby sites (gray solid line) can lead to a change of atom-cavity coupling due to incommensurate lattice (λ_l) and cavity (λ_c) wavelengths. The cavity has a finite linewidth κ . (b) The initially localized Wannier orbitals can also be written as a superposition of partially delocalized Wannier-Stark states which accumulate different phases due to gravity. (c) Frequencies of atomic transition (ω_0), external pump (ω_p), and cavity resonance (ω_c). Due to atomic motion, the cavity resonance will be shifted by $\mathcal{G}_0^2 N_{\text{eff}}(t)/\Delta_0$, with $N_{\text{eff}}(t)$ defined in Eq. (3). (d) $N_{\text{eff}}(t)$ displays oscillatory behavior reflecting single-particle atomic BOs, generated by a sudden quench on lattice depth from $15E_R$ to $8E_R$.

ground manifold, is coupled to an atomic excited state $|e\rangle$ with a transition energy $\hbar\omega_0$ via a single cavity mode \hat{a} with frequency ω_c and wavelength λ_c . The atom-cavity coupling has spatial dependence $\mathcal{G}(z) = \mathcal{G}_0 \sin(k_c z)$, with $k_c = 2\pi/\lambda_c$ and \mathcal{G}_0 is proportional to single-atom vacuum Rabi splitting. The cavity mode is coherently driven by an additional laser with frequency ω_p thus detuning $\Delta_c = \omega_p - \omega_c$ from the bare cavity mode, which generates a net injected field in the cavity with amplitude η_p . The cavity has a finite linewidth κ .

We work in the dispersive regime of the atom-light interaction, where both the cavity mode and the external drive are far detuned from the atomic resonance, i.e., $\Delta_0 \gg \mathcal{G}_0 \sqrt{\langle \hat{a}^\dagger \hat{a} \rangle}$ with $\Delta_0 = \omega_p - \omega_0$. In such limit, we can adiabatically eliminate the excited state and only consider the atomic motion in the ground state, which results in the following second-quantized Hamiltonian,

$$\hat{H} = \hat{H}_0 + \int dz \hat{\psi}_g^\dagger(z) \frac{\hbar |\mathcal{G}(z)|^2}{\Delta_0} \hat{a}^\dagger \hat{a} \hat{\psi}_g(z) + \hat{H}_{\text{cav}}, \quad (1)$$

where $\hat{H}_0 = \int dz \hat{\psi}_g^\dagger [\hat{p}^2/2M + V_0 \sin^2(k_l z) + Mgz] \hat{\psi}_g$ includes the kinetic energy, lattice potential, and gravitational potential experienced by the atoms. Here, V_0 is the lattice depth, and $k_l = 2\pi/\lambda_l$ is the wave number of the lattice beam that sets the atomic recoil energy $E_R = \hbar^2 k_l^2/2M$, where λ_l is the lattice wavelength. The field operator $\hat{\psi}_g(z)$ annihilates a ground state atom at position z . The second term in Eq. (1)

describes the dispersive atom-light coupling after the adiabatic elimination of the excited state. The cavity Hamiltonian is given by $\hat{H}_{\text{cav}}/\hbar = -\Delta_c \hat{a}^\dagger \hat{a} + \eta_p \hat{a}^\dagger + \eta_p^* \hat{a}$.

The eigenstates of \hat{H}_0 are the so-called WS states. In the tight-binding limit, the wave function for a WS state centered at lattice site n takes the form of $\phi_n(z) = \sum_m \mathcal{J}_{m-n}(2J_0/Mga_1) w(z - ma_1)$ [12,33], which is a superposition of localized ground-band Wannier functions $w(z)$ [see Fig. 1(b)]. Here \mathcal{J}_n is the Bessel function of the first kind, J_0/\hbar is the nearest-neighbor tunneling rate, and $a_1 = \lambda_l/2$ is the lattice spacing. The eigenenergy of $|\phi_n\rangle$ is $n\hbar\omega_B$, where $\omega_B = Mga_1/\hbar$ is the Bloch frequency and $T_B = 2\pi/\omega_B$ the corresponding Bloch period. We expand the field operator in the WS basis, $\hat{\psi}_g(z) = \sum_n \hat{c}_n \phi_n(z)$, where the operator \hat{c}_n annihilates an atom in the WS state ϕ_n . In this basis, Eq. (1) can be rewritten as

$$\hat{H} = \hat{H}_{\text{cav}} + \frac{\hbar \mathcal{G}_0^2}{\Delta_0} \hat{a}^\dagger \hat{a} \hat{N}_{\text{eff}} + \hbar\omega_B \sum_n n \hat{c}_n^\dagger \hat{c}_n, \quad (2)$$

where

$$\hat{N}_{\text{eff}} = \sum_{m,n} J_{m,n} \hat{c}_m^\dagger \hat{c}_n. \quad (3)$$

Here, $J_{m,n} = \int dz \phi_m(z) \phi_n(z) \sin^2(k_c z)$ describes the overlap between the WS states ϕ_m, ϕ_n weighted by the cavity field mode function. \hat{N}_{eff} can be understood as the effective number of atoms coupled to the cavity, which are responsible for generating a frequency shift $\mathcal{G}_0^2 N_{\text{eff}}/\Delta_0$ on the cavity resonance, where $N_{\text{eff}} = \langle \hat{N}_{\text{eff}} \rangle$. This dispersive term allows us to either perform nondestructive probing or many-body control of the atomic motion, depending on the operating parameter regime.

Assuming the cavity field adiabatically follows the atomic motion, which is valid since the cavity field dynamics ($\Delta_c \sim \text{MHz}$) is much faster than the time evolution of the atomic field ($\omega_B \sim \text{kHz}$), one can replace the cavity field operator by $\hat{a} \approx \eta_p/(\Delta_c - \mathcal{G}_0^2 \hat{N}_{\text{eff}}/\Delta_0)$. This leads to the following effective atom-only Hamiltonian [32],

$$\hat{H}_{\text{eff}}/\hbar = \omega_B \sum_n n \hat{c}_n^\dagger \hat{c}_n + \hat{V}_{\text{cav}}(\hat{N}_{\text{eff}}), \quad (4)$$

where $\hat{V}_{\text{cav}}(\hat{N}_{\text{eff}}) = -(VN/\beta)/(1 + \beta \hat{N}_{\text{eff}}/N)$ is the cavity-induced potential depending on the atomic motion. Here, $V = \mathcal{G}_0^2 |\eta_p|^2 / (\Delta_c^2 \Delta_0)$ is the maximum ac Stark shift on the atoms introduced by the bare cavity mode, and $\beta = -N\mathcal{G}_0^2 / (\Delta_0 \Delta_c)$ is the ratio between the maximum cavity shift and the bare cavity detuning. We assume $\beta > 0$ (Δ_0 and Δ_c have opposite signs) to avoid hitting a cavity resonance.

III. SINGLE-PARTICLE DYNAMICS

First we consider the simplest case where the cavity is used as a probe and does not affect the single-particle dynamics set by \hat{H}_0 , valid in the regimes $V \ll \omega_B$. We consider the case where atoms are initially loaded in an almost localized WS state in a deep lattice at sites n minimally coupled to the cavity ($k_c n a_1/\pi = r$ with $n, r \in \mathbb{Z}$). Then we suddenly quench the lattice depth to a shallow depth, and the atoms start hopping to the nearest-neighbor sites [see Fig. 1(a)]. Since the initially localized state corresponds to a superposition of WS

states of the shallow lattice [see Fig. 1(b)], after the quench, each WS state acquires a phase that evolves at a rate set by ω_B . The interference of different WS states induces tunneling away from the initially populated site, resulting in coherent breathing behavior at the BO frequency ω_B .

To probe the BO, we use the fact that atoms at different sites coupled differently to the cavity. Therefore tunneling out and back into the initial site leads to a periodic oscillation in $N_{\text{eff}}(t)$ at frequency ω_B as shown in Fig. 1(d), which can be measured by tracking the cavity frequency shift $G_0^2 N_{\text{eff}}(t)/\Delta_0$. Note that a technique to initially prepare atoms at lattice sites with low initial coupling to the cavity mode has been demonstrated in [10]. Instead of an initially localized state, we can also use amplitude modulation of the lattice depth [19] to prepare a superposition of WS states. In this case a similar behavior can be observed as detailed in [32].

For the numerical simulations throughout this Letter, we consider the case of ^{87}Rb atoms with cavity wavelength $\lambda_c = 780$ nm and lattice wavelength $\lambda_l = 532$ nm. However, the discussion can be easily adapted to other types of atoms discussed in the Supplemental Material [32].

IV. DEEP LATTICE REGION

The interplay between single-particle atomic motion and cavity-mediated interactions occurs if $V \sim \omega_B$. Here we focus on the deep lattice regime ($V_0 = 20E_R$) where WS states are almost localized at individual lattice sites. If atoms are prepared at site $n = 0$, and $V > 0$, the differential cavity-induced ac Stark shift (first order in β in the limit $\beta \ll 1$) between the $n = 0$ and $n = -1$ sites $\propto V(J_{0,0} - J_{-1,-1})$ can compensate for their energy difference $\hbar\omega_B$ as shown in Fig. 2(a), restoring tunneling between these two sites. Since the atomic motion is restricted to take place between these two states, we map them to an effective spin-1/2 degree of freedom: \hat{c}_{-1} as \hat{c}_{\uparrow} , \hat{c}_0 as \hat{c}_{\downarrow} as well as the spin operators $\hat{S}_z = (\hat{c}_{\uparrow}^\dagger \hat{c}_{\uparrow} - \hat{c}_{\downarrow}^\dagger \hat{c}_{\downarrow})/2$, $\hat{S}_x = (\hat{c}_{\uparrow}^\dagger \hat{c}_{\downarrow} + \hat{c}_{\downarrow}^\dagger \hat{c}_{\uparrow})/2$. Thus we have $\hat{N}_{\text{eff}} = 2(\Delta_{-1} \hat{S}_z + \Omega_{-1} \hat{S}_x) + N\bar{\omega}$, where $\Delta_{-1} = (J_{-1,-1} - J_{0,0})/2$, $\Omega_{-1} = J_{-1,0}$, and $\bar{\omega} = (J_{-1,-1} + J_{0,0})/2$.

In the limit of $\beta \ll 1$, one can expand \hat{H}_{eff} [Eq. (4)] in a power series of β , and keep only the leading order terms. The Hamiltonian simplifies to

$$\hat{H}_{\text{eff}}/\hbar \approx -\omega_B \hat{S}_z + V \hat{N}_{\text{eff}} - \frac{V\beta}{N} \hat{N}_{\text{eff}}^2. \quad (5)$$

This approximated Hamiltonian [Eq. (5)] is equivalent to the LMG model [12,21–25,32,34], $H_{\text{LMG}} = \chi \hat{S}_z^2 + \tilde{\Omega} \hat{S}_x - \tilde{\delta} \hat{S}_z$, by a rotation along the y axis of the Bloch sphere, $\hat{S}_\alpha = \hat{R}^\dagger \hat{S}_\alpha R$, where $\hat{R} = \exp(i\theta \hat{S}_y)$, and $\tan \theta = \Delta_{-1}/\Omega_{-1}$ [32], which enables fast entanglement state generation under a particular choice of χ , $\tilde{\Omega}$, $\tilde{\delta}$ [23–25]. The LMG model features a DPT from a dynamical ferromagnetic (FM) phase to a dynamical paramagnetic phase (PM), signaled by a sharp change in the behavior of the long-time average of the excitation fraction [21,22]. In our model [Eq. (4)], the long-time average of the signal $\bar{N}_{\text{eff}}/N = \lim_{T \rightarrow \infty} \int_0^T dt N_{\text{eff}}(t)/(TN)$ plays the role of the dynamical order parameter. We also show that the DPT exists in our model [Eq. (4)] even beyond the $\beta \ll 1$ limit as we discuss below.

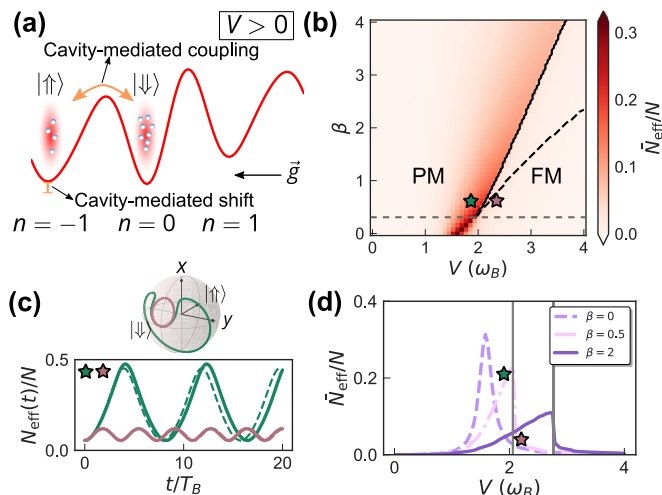


FIG. 2. Dynamical phase transition (DPT) in the deep lattice regime ($V_0 = 20E_R$). (a) For the case of $V > 0$ we define an effective spin-1/2 degrees of freedom: $|\uparrow\rangle$ ($|\phi_{-1}\rangle$) and $|\downarrow\rangle$ ($|\phi_0\rangle$). The cavity-mediated interactions generate energy shifts to balance the potential energy of these two sites (red curve), as well as dynamical couplings between them (orange arrow). (b) Phase diagram of the DPT determined by the long-time average \bar{N}_{eff}/N . The phase boundary separating the paramagnetic (PM) and ferromagnetic (FM) phases is predicted by the full model (solid line) and the LMG model (black dashed line). The smooth crossover regime is below the gray dashed line. (c) Mean-field dynamics with $V = 1.9\omega_B$, $\beta = 0.5$ (green) and $V = 2.2\omega_B$, $\beta = 0.5$ (red). The upper panel shows the mean-field trajectories on the Bloch sphere, and the lower panel displays the normalized signal $N_{\text{eff}}(t)/N$. The solid (dashed) line shows predictions of the full (LMG) model, respectively. (d) Horizontal cut of the phase diagram in (b) for $\beta = 0$ (solid), $\beta = 0.5$ (dashed), and $\beta = 2$ (dot dashed).

To find the DPT, we solve the mean-field equations of motion for $s_{x,y,z} = 2\langle \hat{S}_{x,y,z} \rangle/N$. Such nonlinear dynamics can be further reduced to $(N_{\text{eff}}/N)^2 + f(N_{\text{eff}}/N) = 0$ with $f(J_{0,0}) = 0$, and we can associate the DPT with an abrupt change in the number of real roots of the effective potential $f(N_{\text{eff}}/N)$ [32]. This leads to the distinct dynamical behaviors of N_{eff}/N tuned by varying V and β as shown in Figs. 2(b)–2(d). When the dynamics are dominated by interaction effects, the system is in the FM phase where the Bloch vector features small oscillations around the south pole, also shown as small amplitude oscillations in $N_{\text{eff}}(t)/N$. This phase is separated by a DPT to a PM phase where the Bloch vector exhibits large excursions around the Bloch sphere, also shown as large amplitude oscillations in $N_{\text{eff}}(t)/N$. For $\beta < 0.32$ [32], the DPT transforms into a smooth crossover and the dynamics becomes dominated by single-particle tunneling processes. The dynamical phase boundary is plotted in Fig. 2(b) with the full model (solid line) and the LMG model (dashed line). The LMG model is unable to capture the phase boundary beyond the $\beta \ll 1$ limit.

V. SHALLOW LATTICE REGION

In a shallow lattice, the WS states extend over a few adjacent lattice sites. In this case, one can obtain a significant suppression of differential ac Stark shifts generated by the

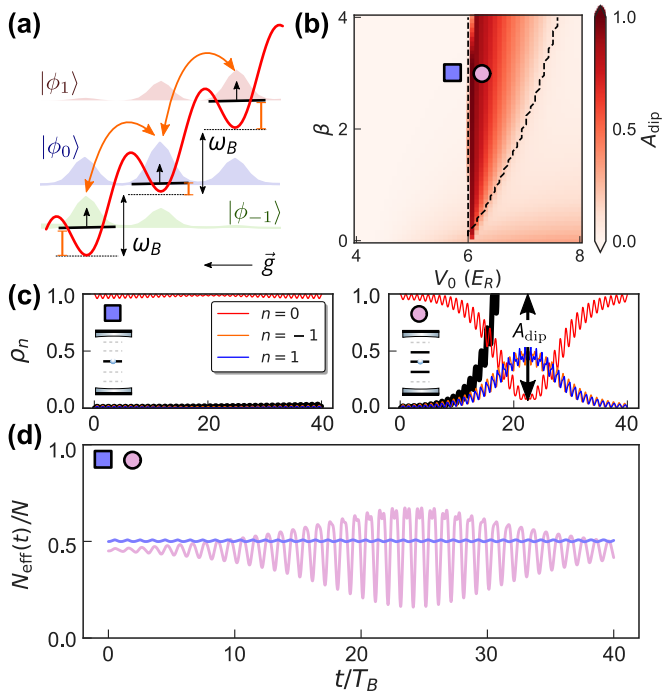


FIG. 3. Cavity-mediated amplification of Bloch oscillations in the shallow lattice regime. (a) The red lines show the gravity plus optical lattice potential. Around $V_0 \approx 6E_R$, WS states can extend to the nearest-neighbor lattice sites. The orange vertical lines represent the cavity-induced on-site shift of the energy levels and the orange arrows illustrate the cavity-mediated tunneling process shown in Eq. (6). (b) Transition between amplification regime and normal regime indicated by $A_{\text{dip}} = 1 - \min\{\rho_0\}$. V is fixed to be $2\omega_B$. The black dashed line shows the predicted boundary from UPA. (c) Mean-field dynamics of ρ_n with initial state $|\phi_0\rangle$ and $V = 2\omega_B$, $\beta = 3$. Nearly no dynamics happen in the left panel (purple square, $V_0 = 5.8E_R$) while a large population transfer to $|\phi_1\rangle$ and $|\phi_{-1}\rangle$ (pink circle, $V_0 = 6.2E_R$) is observed in the right panel. (d) Mean-field simulations for the normalized signal $N_{\text{eff}}(t)/N$ for the same parameters described in (c). The purple line stays almost constant while the pink line signals the cavity enhancement of the BO.

cavity by operating near the so-called magic lattice depth ($V_0 = 6E_R$ for the Rb parameters we use) [12], where $J_{n,n}$ is nearly a constant and the energy difference between nearest-neighbor WS states is roughly $\hbar\omega_B$ [see Fig. 3(a)]. Thus the dynamics features a BO even in the presence of strong cavity-mediated interactions. In fact, after preparing the atoms in the WS state $|\phi_0\rangle$ and thus in an eigenstate of the single-particle Hamiltonian, one can observe the generation and amplification of the BO due to cavity-mediated interactions in a window around the magic depth as shown in Figs. 3(b)–3(d). Since the short-time dynamics occurs mainly between the WS states centered at $n = 0, \pm 1$, we can concentrate only on these states and simplify the dynamics via the undepleted pump approximation (UPA): To the leading order, one can replace the operators for the initially occupied states as c numbers, $\hat{c}_0, \hat{c}_0^\dagger \sim \sqrt{N}$, and keep the operators for unoccupied states ($\hat{c}_{\pm 1}, \hat{c}_{\pm 1}^\dagger$) to the second order while absorbing the linear term generated by single-particle tunneling via a displacement of

a coherent state, $\hat{c}_{\pm 1} = \alpha_{\pm 1} + \hat{c}'_{\pm 1}$. In this way, \hat{H}_{eff} [Eq. (4)] simplifies into a quadratic form [32],

$$\hat{H}_{\text{eff}}/\hbar \approx \omega_B(\hat{c}'_1 \hat{c}'_1 - \hat{c}'_{-1} \hat{c}'_{-1}) + V_1 \Delta(\hat{c}'_1 \hat{c}'_1 + \hat{c}'_{-1} \hat{c}'_{-1}) + V_2 N \Omega^2 (\hat{c}'_1 + \hat{c}'_1 - \hat{c}'_{-1} - \hat{c}'_{-1})^2, \quad (6)$$

with the expansion coefficient V_1, V_2 in [32] and $\Delta = \Delta_1 \approx \Delta_{-1}$, $\Omega = \Omega_1 \approx -\Omega_{-1}$.

We analyze the exact dynamics of Eq. (6) via the Bogoliubov–de Gennes (BdG) method, in which the Heisenberg equation of motion for operators $\hat{C} = (\hat{c}'_1, \hat{c}'_{-1}, \hat{c}'_1, \hat{c}'_{-1})^T$ takes the form $i\partial_t \hat{C} = \mathcal{H}_{\text{BdG}} \hat{C}$. The matrix \mathcal{H}_{BdG} can have either real or complex eigenvalues, which leads to distinct dynamical behaviors as shown in Fig. 3(c). When all the eigenvalues are real (normal regime), the populations ρ_0 and $\rho_{\pm 1}$, with $\rho_n = \langle \hat{c}_n^\dagger \hat{c}_n \rangle$, feature stable small amplitude oscillations; on the other hand, when all the eigenvalues are complex, then $\rho_{\pm 1}$ feature an exponential growth associated with the correlated pair production of atoms at the WS state centered at $n = \pm 1$, which leads to the amplification of the BO signal until the UPA breaks down. The transition between the real and complex eigenvalues of \mathcal{H}_{BdG} is marked by dashed lines in Fig. 3(b).

To quantify the population transfer, we define $A_{\text{dip}} = 1 - \min\{\rho_0\}$ with $\min\{\rho_0\}$ as the minimum of ρ_0 during $t \in [0, 40T_B]$. A large A_{dip} signals efficient population transfer. In Fig. 3(b), we show A_{dip} as a function of the lattice depth V_0 and the cavity parameter β . The region of amplified BO lies within the two dashed boundaries. The left boundary is fixed at the magic lattice depth ($V_0 = 6E_R$) and the right boundary pushes to larger β as V_0 increases. Inside the amplification region $A_{\text{dip}} \neq 0$, while outside $A_{\text{dip}} \approx 0$. The evolution of $N_{\text{eff}}(t)/N$ is shown in Fig. 3(d), where the enhanced population transfer induced by the cavity-mediated interactions lead to the growth of the BO amplitude in the amplification regime.

VI. EXPERIMENTAL CONSIDERATION

The predicted behavior should be achievable in state-of-the-art cavity QED systems with $N \sim 10^4$ ^{87}Rb atoms. We focus on the unitary dynamics in this Letter while the main decoherence sources come from cavity loss and spontaneous emission from the excited states. The cavity loss generates collective dephasing processes at a rate $V\beta\kappa/\Delta_c$ and spontaneous emission generates off-resonant photon scattering processes at a rate $V\gamma/\Delta_0$, where γ is the spontaneous emission rate. For an optical cavity with cooperativity $C = 4\mathcal{G}_0^2/\gamma\kappa \sim 0.5$, $\kappa/\Delta_c \sim 0.05$, $\gamma/\Delta_0 \sim 0.01$, one obtains negligible dissipation within experimentally relevant timescales (~ 50 BO periods). Our scheme does not require BEC while it utilizes site selection to prepare the initial state, which is robust to the radial thermal noise up to $T \sim 1 \mu\text{K}$ [32]. Contact interactions between atoms can also be ignored for the dilute quantum gas used here (~ 50 atoms per site). Moreover, our model can be realized with other species of alkali-metal atoms (D_2 transition) and alkaline-earth-metal atoms ($^1S_0 \rightarrow ^3P_1$ transition) with appropriate choices of lattice wavelength [32]. In particular, contact interactions can be further suppressed using ^{88}Sr atoms featuring negligible scattering lengths or

any type of fermionic atoms interacting only via the p -wave channel.

VII. CONCLUSION AND OUTLOOK

In summary, we proposed a scheme to perform many-body control of atomic BOs in an optical cavity. Our work opens up possibilities for Hamiltonian engineering in many-body systems by taking advantage of the interplay between atomic motion, gravity, and cavity-mediated interactions. For example, although so far we only focused on a single internal level, by including more levels and more cavity modes, it should be possible to engineer dynamical self-generated couplings between WS states via cavity-mediated interactions, which could be used to study dynamical gauge field [35–37] in a synthetic ladder without the overhead of Raman beams. Furthermore, although most of the calculations so far have been limited to regimes where the mean-field dynamics are a

good description of the system, by loading the atoms in a two-dimensional or three-dimensional lattice, one should be able to increase the role of beyond mean-field effects and enter the regimes where quantum correlations dominate the dynamics.

ACKNOWLEDGMENTS

We thank Tianrui Xu and Tobias Bothwell for critical reading of the manuscript, and we thank Helmut Ritsch for useful discussions. This work is supported by the U.S. Department of Energy, Office of Science, National Quantum Information Science Research Centers, Quantum Systems Accelerator. Additional support is acknowledged from by the DARPA (funded via ARO) Grant No. W911NF-16-1-0576, the ARO single investigator Grant No. W911NF-19-1-0210, the NSF PHY1820885, NSF JILA-PFC PHY-1734006 and NSF QLCI-2016244 grants and by NIST.

-
- [1] F. Bloch, Über die quantenmechanik der elektronen in kristallgittern, *Z. Phys.* **52**, 555 (1929).
 - [2] C. Waschke, H. G. Roskos, R. Schwedler, K. Leo, H. Kurz, and K. Köhler, Coherent Submillimeter-Wave Emission from Bloch Oscillations in a Semiconductor Superlattice, *Phys. Rev. Lett.* **70**, 3319 (1993).
 - [3] M. Ben Dahan, E. Peik, J. Reichel, Y. Castin, and C. Salomon, Bloch Oscillations of Atoms in an Optical Potential, *Phys. Rev. Lett.* **76**, 4508 (1996).
 - [4] B. P. Anderson and M. A. Kasevich, Macroscopic quantum interference from atomic tunnel arrays, *Science* **282**, 1686 (1998).
 - [5] H. Keßler, J. Klinder, B. P. Venkatesh, C. Georges, and A. Hemmerich, *In situ* observation of optomechanical Bloch oscillations in an optical cavity, *New J. Phys.* **18**, 102001 (2016).
 - [6] C. Georges, J. Vargas, H. Keßler, J. Klinder, and A. Hemmerich, Bloch oscillations of a Bose-Einstein condensate in a cavity-induced optical lattice, *Phys. Rev. A* **96**, 063615 (2017).
 - [7] B. M. Peden, D. Meiser, M. L. Chiofalo, and M. J. Holland, Nondestructive cavity QED probe of Bloch oscillations in a gas of ultracold atoms, *Phys. Rev. A* **80**, 043803 (2009).
 - [8] B. Prasanna Venkatesh, M. Trupke, E. A. Hinds, and D. H. J. O’Dell, Atomic Bloch-Zener oscillations for sensitive force measurements in a cavity, *Phys. Rev. A* **80**, 063834 (2009).
 - [9] B. P. Venkatesh and D. H. J. O’Dell, Bloch oscillations of cold atoms in a cavity: Effects of quantum noise, *Phys. Rev. A* **88**, 013848 (2013).
 - [10] B. Wu, G. P. Greve, C. Luo, and J. K. Thompson, Site-dependent selection of atoms for homogeneous atom-cavity coupling, *arXiv:2104.01201*.
 - [11] R. D. Niederriter, C. Schlupf, and P. Hamilton, Cavity probe for real-time detection of atom dynamics in an optical lattice, *Phys. Rev. A* **102**, 051301(R) (2020).
 - [12] A. Chu, P. He, J. K. Thompson, and A. M. Rey, Quantum Enhanced Cavity QED Interferometer with Partially Delocalized Atoms in Lattices, *Phys. Rev. Lett.* **127**, 210401 (2021).
 - [13] A. Buchleitner and A. R. Kolovsky, Interaction-Induced Decoherence of Atomic Bloch Oscillations, *Phys. Rev. Lett.* **91**, 253002 (2003).
 - [14] A. R. Kolovsky, New Bloch Period for Interacting Cold Atoms in 1D Optical Lattices, *Phys. Rev. Lett.* **90**, 213002 (2003).
 - [15] D. Witthaut, M. Werder, S. Mossmann, and H. J. Korsch, Bloch oscillations of Bose-Einstein condensates: Breakdown and revival, *Phys. Rev. E* **71**, 036625 (2005).
 - [16] T. Schulte, S. Drenkelforth, G. K. Büning, W. Ertmer, J. Arlt, M. Lewenstein, and L. Santos, Dynamics of Bloch oscillations in disordered lattice potentials, *Phys. Rev. A* **77**, 023610 (2008).
 - [17] S. Walter, D. Schneble, and A. C. Durst, Bloch oscillations in lattice potentials with controlled aperiodicity, *Phys. Rev. A* **81**, 033623 (2010).
 - [18] F. Meinert, M. J. Mark, E. Kirilov, K. Lauber, P. Weinmann, M. Gröbner, and H.-C. Nägerl, Interaction-Induced Quantum Phase Revivals and Evidence for the Transition to the Quantum Chaotic Regime in 1D Atomic Bloch Oscillations, *Phys. Rev. Lett.* **112**, 193003 (2014).
 - [19] A. Alberti, G. Ferrari, V. V. Ivanov, M. L. Chiofalo, and G. M. Tino, Atomic wave packets in amplitude-modulated vertical optical lattices, *New J. Phys.* **12**, 065037 (2010).
 - [20] L. Masi, T. Petrucciani, G. Ferioli, G. Semeghini, G. Modugno, M. Inguscio, and M. Fattori, Spatial Bloch Oscillations of a Quantum Gas in a “Beat-Note” Superlattice, *Phys. Rev. Lett.* **127**, 020601 (2021).
 - [21] A. Chu, J. Will, J. Arlt, C. Klempt, and A. M. Rey, Simulation of XXZ Spin Models Using Sideband Transitions in Trapped Bosonic Gases, *Phys. Rev. Lett.* **125**, 240504 (2020).
 - [22] J. A. Muniz, D. Barberena, R. J. Lewis-Swan, D. J. Young, J. R. K. Cline, A. M. Rey, and J. K. Thompson, Exploring dynamical phase transitions with cold atoms in an optical cavity, *Nature (London)* **580**, 602 (2020).
 - [23] J. Ma, X. Wang, C.-P. Sun, and F. Nori, Quantum spin squeezing, *Phys. Rep.* **509**, 89 (2011).
 - [24] L. Pezzè, A. Smerzi, M. K. Oberthaler, R. Schmied, and P. Treutlein, Quantum metrology with nonclassical states of atomic ensembles, *Rev. Mod. Phys.* **90**, 035005 (2018).
 - [25] Z. Li, S. Colombo, C. Shu, G. Velez, S. Pilatowsky-Cameo, R. Schmied, S. Choi, M. Lukin, E. Pedrozo-Peñafiel, and

- V. Vuletić, Improving metrology with quantum scrambling, *Science* **380**, 1381 (2023).
- [26] C. Gross, H. Strobel, E. Nicklas, T. Zibold, N. Bar-Gill, G. Kurizki, and M. Oberthaler, Atomic homodyne detection of continuous-variable entangled twin-atom states, *Nature (London)* **480**, 219 (2011).
- [27] B. Lücke, M. Scherer, J. Kruse, L. Pezzé, F. Deuretzbacher, P. Hyllus, O. Topic, J. Peise, W. Ertmer, J. Arlt *et al.*, Twin matter waves for interferometry beyond the classical limit, *Science* **334**, 773 (2011).
- [28] A. Periwal, E. S. Cooper, P. Kunkel, J. F. Wienand, E. J. Davis, and M. Schleier-Smith, Programmable interactions and emergent geometry in an array of atom clouds, *Nature (London)* **600**, 630 (2021).
- [29] F. Finger, R. Rosa-Medina, N. Reiter, P. Christodoulou, T. Donner, and T. Esslinger, Spin-and momentum-correlated atom pairs mediated by photon exchange, [arXiv:2303.11326](https://arxiv.org/abs/2303.11326)
- [30] C. D. Panda, M. Tao, J. Egelhoff, M. Ceja, V. Xu, and H. Müller, Quantum metrology by one-minute interrogation of a coherent atomic spatial superposition, [arXiv:2210.07289](https://arxiv.org/abs/2210.07289).
- [31] C. Luo, H. Zhang, V. P. Koh, J. D. Wilson, A. Chu, M. J. Holland, A. M. Rey, and J. K. Thompson, Cavity-mediated collective momentum-exchange interactions, [arXiv:2304.01411](https://arxiv.org/abs/2304.01411).
- [32] See Supplemental Material at <http://link.aps.org/supplemental/10.1103/PhysRevResearch.5.L032039> for details of effective Hamiltonian derivation, dynamical phase transition, undepleted pump approximation, and experimental implementation, includes Refs. [12,19,21,22,38].
- [33] M. Glück, A. R. Kolovsky, and H. J. Korsch, Wannier-Stark resonances in optical and semiconductor superlattices, *Phys. Rep.* **366**, 103 (2002).
- [34] A. Aeppli, A. Chu, T. Bothwell, C. J. Kennedy, D. Kedar, P. He, A. M. Rey, and J. Ye, Hamiltonian engineering of spin-orbit-coupled fermions in a Wannier-Stark optical lattice clock, *Sci. Adv.* **8**, eadc9242 (2022).
- [35] F. Mivehvar, F. Piazza, T. Donner, and H. Ritsch, Cavity QED with quantum gases: new paradigms in many-body physics, *Adv. Phys.* **70**, 1 (2021).
- [36] E. Colella, A. Kosior, F. Mivehvar, and H. Ritsch, Open Quantum System Simulation of Faraday’s Induction Law via Dynamical Instabilities, *Phys. Rev. Lett.* **128**, 070603 (2022).
- [37] R. Rosa-Medina, F. Ferri, F. Finger, N. Dogra, K. Kroeger, R. Lin, R. Chitra, T. Donner, and T. Esslinger, Observing Dynamical Currents in a Non-Hermitian Momentum Lattice, *Phys. Rev. Lett.* **128**, 143602 (2022).
- [38] K. C. Cox, G. P. Greve, B. Wu, and J. K. Thompson, Spatially homogeneous entanglement for matter-wave interferometry created with time-averaged measurements, *Phys. Rev. A* **94**, 061601(R) (2016).